PNAS RESEARCH ARTICLE | PLANT BIOLOGY

COP1 controls light-dependent chromatin remodeling

Wenli Wang[a], Junghyun Kim[a], Teresa S. Martinez[a], Enamul Huq[a], and Sibum Sung[a,1]

Edited by David Baulcombe, University of Cambridge, Cambridge, United Kingdom; received July 26, 2023; accepted January 3, 2024

Light is a crucial environmental factor that impacts various aspects of plant development. Phytochromes, as light sensors, regulate myriads of downstream genes to mediate developmental reprogramming in response to changes in environmental conditions. CONSTITUTIVELY PHOTOMORPHOGENIC 1 (COP1) is an E3 ligase for a number of substrates in light signaling, acting as a central repressor of photomorphogenesis. The interplay between phytochrome B (phyB) and COP1 forms an antagonistic regulatory module that triggers extensive gene expression reprogramming when exposed to light. Here, we uncover a role of COP1 in light-dependent chromatin remodeling through the regulation of VIL1 (VIN3-LIKE 1)/VERNALIZATION 5, a Polycomb protein. VIL1 directly interacts with phyB and regulates photomorphogenesis through the formation of repressive chromatin loops at downstream growth-promoting genes in response to light. Furthermore, we reveal that COP1 governs light-dependent formation of chromatin loop and limiting a repressive histone modification to fine-tune expressions of growth-promoting genes during photomorphogenesis through VIL1.

photomorphogenesis | CONSTITUTIVELY PHOTOMORPHOGENIC 1 | VIN3-LIKE 1 | ubiquitin/26S proteosome system | Polycomb

Significance

COP1, an E3 ligase, plays a pivotal role in the regulation of photomorphogenesis in plants. This role is accomplished through its capacity to target and degrade various nuclear substrates via the ubiquitin/26S proteasome system. In this study, we show that COP1 controls global levels of H3K27me3, a histone modification associated with gene repression, through its interaction with a Polycomb protein called VIL1. In the absence of light, COP1 facilitates the degradation of VIL1, subsequently influencing the VIL1-dependent chromatin loop upon exposure to light, thereby modulating the genome-wide level of H3K27me3. This work represents an example in which COP1 directly regulates a chromatin regulator to orchestrate photomorphogenesis.

Light and temperature are two key environmental factors that influence diverse developmental processes throughout the entire life cycle of plants. CONSTITUTIVELY PHOTOMORPHOGENIC 1 (COP1) is a RING-finger protein containing WD40-repeats and a coiled-coil domain and is highly conserved from plants to mammals (1). It is one of the best-characterized E3 ubiquitin ligases with broad roles, including as a central repressor of light signaling in plants and as a tumor suppressor in mammals (1–6). In the nucleus, COP1 interacts with SUPPRESSOR OF PHYA-105 (SPA) proteins to form E3 ligase complexes (7–9) and targets nuclear-localized photomorphogenesis-promoting factors mainly in the dark (5, 10). Upon light exposure, light-activated phytochrome B (phyB) interacts with SPA1 protein and interferes with the formation of COP1-SPA protein complexes to promote photomorphogenesis (11, 12). Light also triggers nuclear exclusion of COP1 through an unknown mechanism (13). COP1 degrades its target proteins through the ubiquitin/26S proteasome system (UPS) (6, 14).

In *Arabidopsis*, a plant homeodomain (PHD) finger-containing protein, VERNALIZATION INSENSITIVE 3 (VIN3), is induced by long-term winter cold, during a process known as vernalization, and triggers the epigenetic repression of *FLOWERING LOCUS C* (*FLC*) by mediating histone modifications at *FLC* chromatin (15). A related PHD finger-containing protein, VIL1/VRN5, was identified in a Yeast-Two Hybrid (Y2H) screen for proteins that interact with VIN3 (16) and also by a genetic screen to identify mutants that impair the vernalization-mediated *FLC* repression (17). As a facultative component of Polycomb Repressive Complex 2 (PRC2), VIL1 functions together with VIN3 in the vernalization-mediated repression of *FLC* by enhancing several histone modifications, including Histone H3 Lys 27 trimethylation (H3K27me3) (16, 18). Unlike *VIN3*, which is only induced by long-term cold, the expression of *VIL1* is not restricted to the period of cold exposure (16, 18), implicating broader roles of VIL1. Indeed, VIL1 functions in various biological processes through its role in promoting the PRC2 activity. VIL1 limits the expressions of *ABSCISIC ACID INSENSITIVE 3 (ABI3)* and *ABSCISIC ACID INSENSITIVE 4 (ABI4)* in the ABA signaling pathway (19), mediates warm temperature responses (20) and contributes to dampening growth-promoting genes during photomorphogenesis (21). In particular, VIL1 directly interacts with the active form of phyB to trigger the formation of a light-dependent chromatin loop facilitating the repression of growth-promoting genes, providing another layer of phytochromes (phys)-mediated gene regulation during photomorphogenesis (21).

Over the last several decades, extensive genetic and biochemical studies have identified numerous substrates of COP1, including various photomorphogenesis-promoting transcription factors and photoreceptors (6, 22–24). Recent studies recognized that multiple layers of chromatin regulation also contribute to light-signaling pathways (21, 25, 26). However, the role of COP1, a central repressor of photomorphogenesis, in the regulation

Author affiliations: [a]Department of Molecular Biosciences, The University of Texas at Austin, Austin, TX 78712

Author contributions: W.W., J.K., E.H., and S.S. designed research; W.W., J.K., and T.S.M. performed research; W.W., J.K., T.S.M., and E.H. contributed new reagents/analytic tools; W.W. and J.K. analyzed data; and W.W. and S.S. wrote the paper.

The authors declare no competing interest.

This article is a PNAS Direct Submission.

[1]To whom correspondence may be addressed. Email: sbsung@austin.utexas.edu.

This article contains supporting information online at https://www.pnas.org/lookup/suppl/doi:10.1073/pnas.2312853121/-/DCSupplemental.

Published February 13, 2024.

of chromatin remodeling in light signaling is not known. In this study, we show that COP1 directly targets and degrades VIL1 through the UPS in the dark, restricting the formation of a light-dependent repressive chromatin loop by VIL1 and thus preventing the PRC2 activity at growth-promoting genes in the dark.

Results

VIL1 Is Unstable and Degraded by the UPS in the Dark. To interrogate the behavior of VIL1 protein under light and dark conditions, we conducted immunoblot assays using the myc-tagged VIL1 complementation line (21). VIL1-myc protein accumulated in response to light and reached a peak after several hours of light irradiation (*SI Appendix*, Fig. S1 *A* and *B*). On the other hand, VIL1-myc protein is degraded in response to the dark treatments (*SI Appendix*, Fig. S1 *C* and *D*). Four-day-old seedlings grown in continuous light were transferred to dark for various periods of time (4, 8, and 24 h) or kept in continuous dark (*SI Appendix*, Fig. S1*C*). Similar to other photomorphogenesis-promoting factors (27, 28), VIL1-myc protein undergoes rapid degradation in the dark and is barely detectable under continuous dark (*SI Appendix*, Fig. S1 *C* and *D*). To address whether VIL1 is degraded through the UPS, we treated 4-d-old *gVIL1*-myc transgenic seedlings with bortezomib (BORTZ), an efficient inhibitor of 26S proteasomes (29). The BORTZ treatment strongly inhibited the degradation of VIL1-myc in the dark, indicating that VIL1 is degraded by the UPS (Fig. 1 *A* and *B*). This prompted us to examine the in vivo ubiquitination levels of VIL1 under the dark and light conditions. Consistent with the degradation through the UPS in the dark, the ubiquitination level of VIL1-myc is higher in darkness than in light (Fig. 1*C*), supporting that VIL1 protein degradation in the dark is poly-ubiquitination-dependent.

COP1 Mediates the Ubiquitination of VIL1. Many photomorphogenesis-promoting factors are subject to COP1-dependent UPS. Therefore, we first assessed whether COP1 mediates the ubiquitination of VIL1 by introgressing VIL1-myc into the *cop1-4* mutant background. Four-day-old dark-grown seedlings were pretreated with BORTZ for 4 h in darkness and then kept in the dark for additional 4 h. The level of VIL1 ubiquitination is drastically reduced in the *cop1-4* background (Fig. 1*D*), indicating that the VIL1 ubiquitination is COP1-dependent. We then evaluated whether the VIL1-myc protein level is also regulated by COP1. Indeed, the levels of VIL1-myc protein are more abundant in the *cop1-4* mutant background under dark conditions (*SI Appendix*, Fig. S1 *E* and *F*). Even in extended dark periods, the level of VIL1 was maintained (Fig. 1 *E* and *F*), showing that COP1 is necessary for the degradation of VIL1 in the dark. In addition, we were able to reconstitute the trans-ubiquitination activity of COP1 to VIL1 in vitro (*SI Appendix*, Fig. S1*G*). Taken together, our results show that COP1 is the E3 ligase of VIL1 and mediates its ubiquitination and degradation through the UPS.

To address the biological significance of VIL1 degradation by COP1 in the dark, we evaluated double mutants of *vil1* and *cop1*. The *vil1* mutant partially suppresses the constitutively photomorphogenic phenotypes (i.e., extremely short hypocotyl) of both *cop1-4* (Fig. 2 *A* and *B*) and *cop1-6* alleles (*SI Appendix*, Fig. S2 *A* and *B*) in the dark. Partial suppression of *cop1* mutants by the *vil1* mutant is observed regardless of growth temperatures (*SI Appendix*, Fig. S2 *C* and *D*). The *cop1* mutants consistently display extremely short hypocotyls under both short-day (sd) and long-day (ld) conditions, but the *vil1* mutant significantly increases the hypocotyl length of *cop1* mutants (*SI Appendix*, Fig. S3 *A–D*). The suppression of the *cop1* mutants by the *vil1* mutant under different photoperiods is observed irrespective of growth temperatures (*SI Appendix*, Fig. S3 *A–D*). *cop1-4* mutants also exhibit various growth phenotypes, including the smaller stature of plants grown in soil (30) (*SI Appendix*, Fig. S4*A*). However, *vil1-1cop1-4* double mutants have larger rosette diameters and larger leaf areas than those in the *cop1-4* mutant (*SI Appendix*, Fig. S4 *A–C*). Taken together, our genetic analyses indicate that *COP1* controls growth in part through *VIL1*.

COP1 Directly Interacts with VIL1 In Vitro and In Vivo. This led us to test whether VIL1 is a bona fide substrate of COP1 by further examining their physical interactions. First, we performed in vitro pull-down assays using MBP-tagged COP1 and GST-tagged VIL1 proteins expressed in *E. coli*. In pull-down assays, recombinant COP1 protein is able to directly interact with VIL1 recombinant protein in vitro (Fig. 2*C*). We, then, employed the split luciferase complementation assay by transiently expressing both proteins in *N. benthamiana* to test *in planta* interaction of COP1 and VIL1. Each split luciferase protein was conjugated with COP1 (COP1–nLuc) and VIL1 (VIL1–cLuc), which generated strong luciferase activity compared with the negative controls (Fig. 2*D*). Furthermore, co-immunoprecipitation (co-IP) assays with transiently expressed VIL1-Flag and COP1-GFP in *N. benthamiana* leaves show the physical interaction between COP1 and VIL1 in planta (Fig. 2*E*). To demonstrate further that VIL1 protein interacts with COP1 in vivo, we performed co-IP, using protein extracts from VIL1-myc complementation transgenic seedlings grown in the dark and treated with BORTZ to ensure the presence of both COP1 and VIL1 proteins. Indeed, we were able to observe that VIL1-myc co-immunoprecipitated with COP1 using anti-COP1 antibody (27) (Fig. 2*F*).

The in vitro binding assay (Fig. 2*C*) pointed out that COP1 and VIL1 directly interact. In addition, Y2H assays confirmed that VIL1 can directly interact with COP1 (*SI Appendix*, Fig. S5 *A* and *B*). The N terminus of COP1 (1–282) comprising the zinc-binding RING domain (Zn), the helical coiled-coil (Coil) domain (*SI Appendix*, Fig. S5*C*) is indispensable for the function of COP1 and is known to interact with numerous substrates of COP1 (28, 31). Our domain-mapping analyses using Y2H identified the N terminus of COP1 (1–282) is mainly responsible for the interaction with VIL1 (*SI Appendix*, Fig. S5*C*). VIL1 is previously known to directly interact with VIN3 through the C-terminal VIN3-interacting domain (16) (VID; *SI Appendix*, Fig. S5*D*). However, the N-terminal fragment of VIL1 including the PHD domain displayed a more robust interaction with COP1 (*SI Appendix*, Fig. S5*D*), indicating that the N terminus of VIL1 interacts with the N terminus of COP1. Taken together, our results show that VIL1 is a substrate of COP1, and the direct interaction between COP1 and VIL1 in the dark leads to the degradation of VIL1 through the UPS.

phyB Is Not Required for the COP1-Mediated Degradation of VIL1. Our previous study showed that VIL1 forms a complex with the active form of phyB in the light (21). Therefore, we tested whether the regulation of VIL1 by COP1 is affected by phyB in vivo. First, we evaluated photomorphogenesis phenotypes of different genotypes (*SI Appendix*, Fig. S6 *A* and *B*). *vil1-1phyB* double mutants exhibit longer hypocotyls, but *vil1-1phyBcop1-4* triple mutant shows a phenotype similar to *vil1-1cop1-4* double mutant, suggesting that the genetic interaction between *COP1*

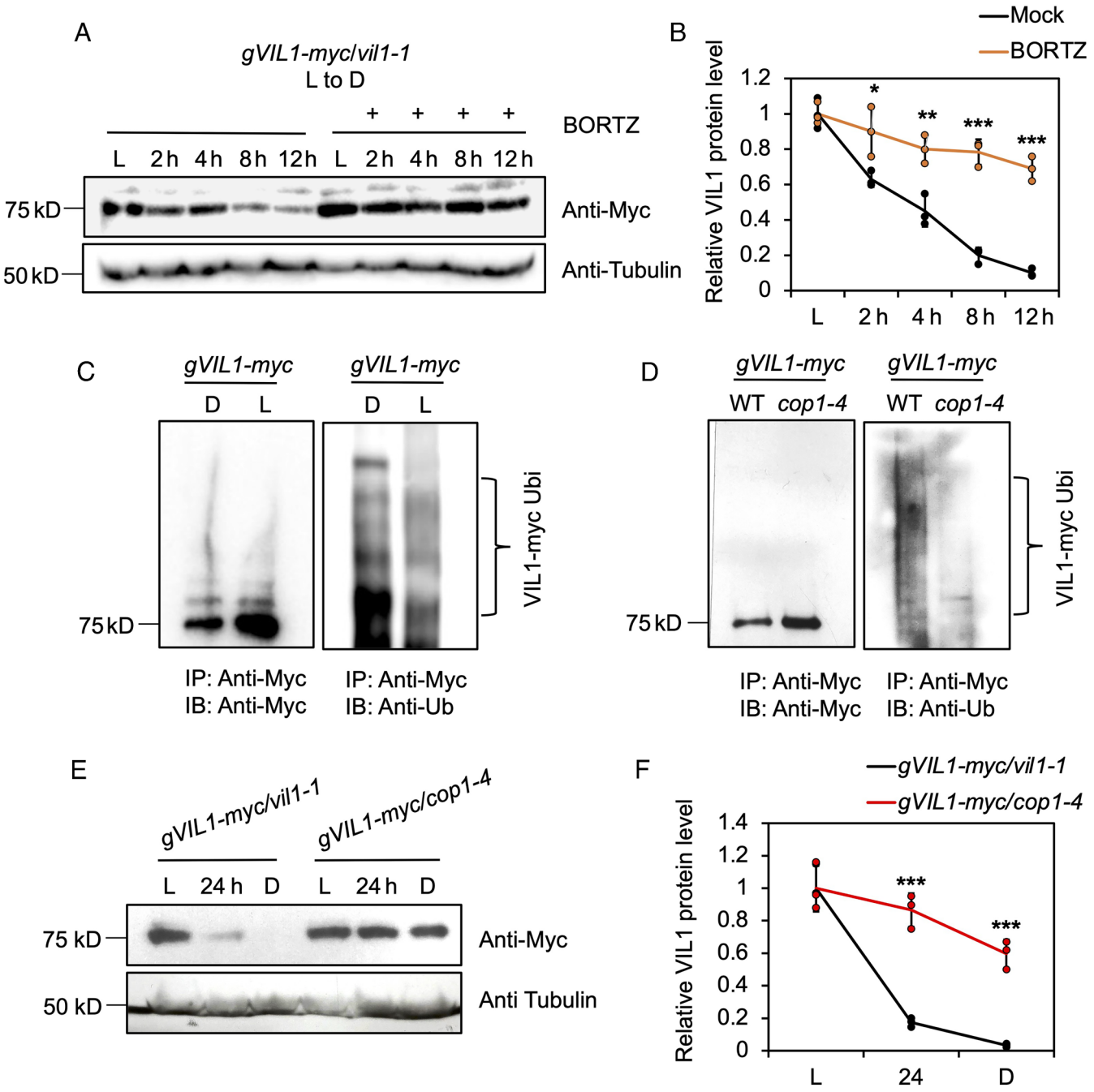

Fig. 1. COP1 mediates VIL1 degradation by the UPS in the dark. (*A*) Treatment with the 26S proteasome inhibitor BORTZ greatly postponed the degradation of VIL1 in the dark. Four-day-old VIL1 transgenic seedlings were treated with or without 40 μM BORTZ after transferring to dark. Samples were collected at the indicated time points. Tubulin was used as an internal control. (*B*) A line graph shows the relative rate of degradation of VIL1 in response to the dark with or without BORTZ treatment. The band intensities of VIL1 and Tubulin were measured using the ImageJ tool. For each line, the VIL1 level in the light (L) was set to 1, and the relative VIL1 levels in response to dark were then calculated. Three independent biological repeats were performed. Error bars represent standard deviation (SD) ($n = 3$). The asterisks indicate statistical differences in a two-tailed Student *t* test (*$P < 0.05$, **$P < 0.01$, and ***$P < 0.001$). (*C*) Immunoblots showing the relative ubiquitination status of VIL1-myc in response to dark and light. (*D*) Immunoblots showing the relative ubiquitination status of VIL1-myc in response to dark in *cop1-4* mutant and WT backgrounds. Total proteins were extracted from 4-d-old dark-grown seedlings and then immunoprecipitated with anti-Myc antibodies. The immunoprecipitated samples were then separated on 7% SDS-PAGE gels and probed with anti-Myc (*Left*) or anti-Ubi antibodies (*Right*). The upper smear bands are polyubiquitinated VIL1. (*E*) Western blots show that VIL1 is degraded at a slower rate in *cop1-4* mutants compared to the WT background. Four-day-old light-grown seedlings (L) were incubated in the dark for 24 h, or seedlings were grown in the dark for 4 d (*D*). (*F*) Quantification of VIL1 levels according to (*E*) using Western blot results from three independent experiments. Tubulin blots were used for normalization. The error bars indicate SD ($n = 3$). The asterisks indicate statistical differences in a two-tailed Student *t* test (***$P < 0.001$). The VIL1 level in the light was set to 1 for each blot.

and *VIL1* may be independent of phyB (*SI Appendix*, Fig. S6 *A* and *B*). In addition, VIL1 degradation in *phyB* mutant still occurs in the dark (*SI Appendix*, Fig. S6 *C* and *D*) but is impaired in the *phyBcop1-4* double mutant background (*SI Appendix*, Fig. S6 *C* and *D*). Furthermore, VIL1 co-immunoprecipitated with COP1 in the *phyB* mutant background (*SI Appendix*, Fig. S6*E*), demonstrating that the interaction between VIL1 and COP1 is little affected by the absence of phyB. These results indicate that phyB is not essential for the interaction between VIL1 and COP1 and COP1-dependent degradation of VIL1.

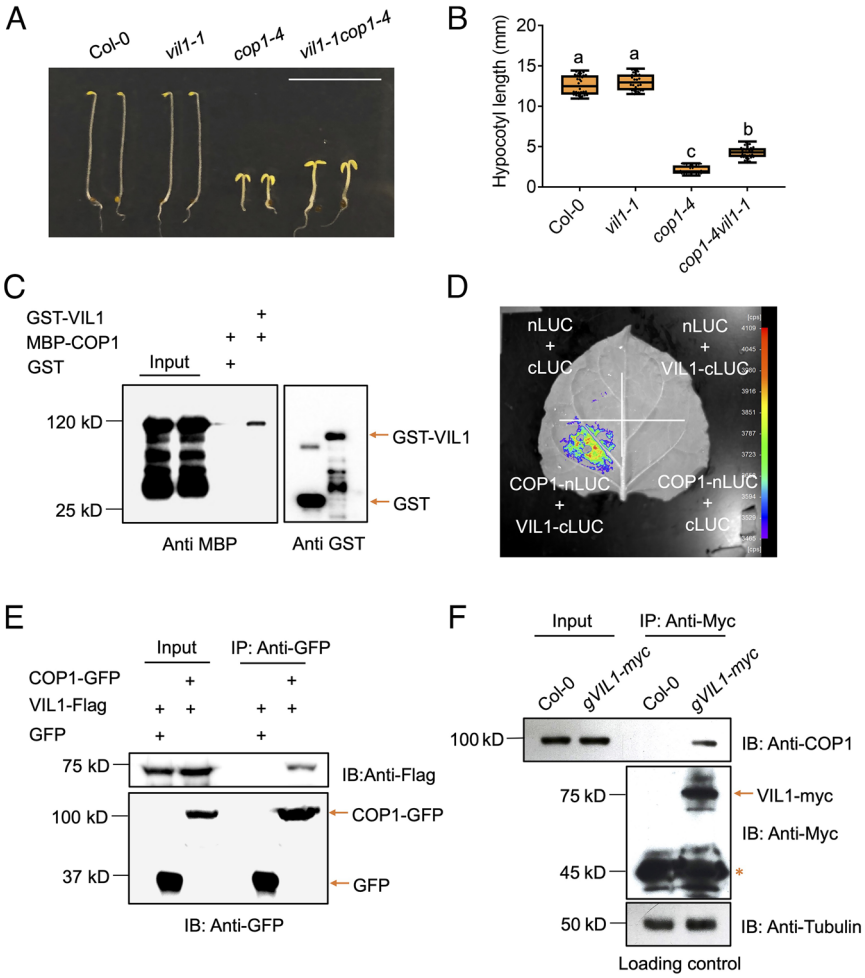

Fig. 2. VIL1 interacts with COP1 both in vitro and in vivo. (*A*) Photograph showing the seedling phenotypes of different genotypes of *Arabidopsis* grown in darkness for 4 d. (Bar, 10 mm.) (*B*) A box plot shows the hypocotyl length of corresponding genotypes grown under the dark for 4 d. Error bars indicate SD ($n > 30$). The letters "a" to "c" indicate statistically significant differences among means of hypocotyl lengths of the genotypes shown based on the one-way ANOVA followed by Tukey's honestly significant difference (HSD) test ($P < 0.05$). (*C*) In vitro pull-down assay shows that GST-VIL1 interacts with MBP-COP1. MBP-COP1 was pulled down by GST-VIL1 using glutathione agarose beads. The pellet fraction was eluted and analyzed by immunoblotting using anti-MBP and anti-GST antibodies. Recombinant maltose-binding protein (MBP)-COP1 and glutathione S-transferase (GST)-VIL1 proteins were purified from *Escherichia coli.* (*D*) Split luciferase complementation assays between VIL1 and COP1 proteins in *Nicotiana benthamiana*. An arrow indicates GST-VIL1 protein or GST protein. (*E*) In vivo co-IP assays show VIL1 protein interacts with COP1. The total proteins extracted from *N. benthamiana* transiently expressed FLAG-tagged VIL1 and GFP-tagged COP1. Plants were grown at 22 °C in LD for additional 3 d after the infiltration. An arrow indicates COP1-GFP protein or GFP protein. (*F*) In vivo co-IP assays show VIL1 protein interacts with COP1. VIL1-myc/*vil1-1* seedlings were grown at 22 °C in the continuous dark for 4 d and then treated with 40 μM BORTZ for at least 4 h. The total proteins were extracted and incubated with protein G beads bound with anti-Myc (mouse) antibody. The total and precipitated proteins were examined by immunoblotting using antibodies against COP1 (rabbit), Myc and Tubulin (mouse). An arrow indicates VIL1-myc protein. The asterisk indicates nonspecific bands. Col-0 was used as a negative control.

The COP1-VIL1 Regulatory Module Mediates the Expression of Growth-Promoting Genes. phyB perceives light signals to promote light responses, whereas COP1 functions as a central repressor to inhibit light responses (7, 8). To evaluate the effect of COP1 on the VIL1-mediated regulation of gene expression, we performed transcriptome analysis of *vil1-1, cop1-4,* and *vil1-1cop1-4* double mutants collected in the dark (ZT0) under the SD condition (*SI Appendix*, Fig. S7*A* and Dataset S1). We identified a large number (~14,000) of genes that exhibit differential expression in the *cop1-4* mutant compared to the wild-type (WT), Col-0 (*SI Appendix*, Fig. S7*A*). To evaluate the gene regulation by COP1 and VIL1, we performed the hierarchical cluster analysis using ~14,000 differentially expressed genes (DEGs) identified in the *cop1-4* mutant (*SI Appendix*, Fig. S7 *B* and *C* and Dataset S2). We found that genes within clusters 1, 4, 6, 8, and 9 (a total of 3,745 genes) show strong repression in the *cop1* mutant but are de-repressed in the *vil1* mutant and in the *vil1-1cop1-4* double mutant (*SI Appendix*, Fig. S7 *B* and *C* and Dataset S2), aligning with the observed phenotypes of corresponding mutants (Fig. 2 *A* and *B* and *SI Appendix*, Figs. S2–S4). This group of genes includes *ATHB2*, a growth-promoting gene that is previously shown to be regulated by *VIL1* (21).

COP1 Controls the Genome-Wide Level of H3K27me3 through VIL1. The *ATHB2* locus is decorated with H3K27me3 in a VIL1-dependent manner, creating repressive chromatin landscapes (21). To address the contribution of COP1 to VIL1-mediated H3K27me3, we performed chromatin immunoprecipitation followed by sequencing (ChIP-seq) in *vil1-1*, *cop1-4,* and *vil1-1cop1-4* mutants (*SI Appendix*, Fig. S8). Consistent with the role of VIL1 in PRC2-mediated H3K27me3 deposition, the genome-wide level of H3K27me3 is lower in *vil1-1* mutants (Fig. 3*A*). Interestingly, we also observed a slight but clear increase ($P = 8.5e^{-4}$) in the level of H3K27me3 in the *cop1-4* mutant compared to the WT at a genomic level, indicating that COP1 affects global-level of H3K27me3 enrichment. This increase

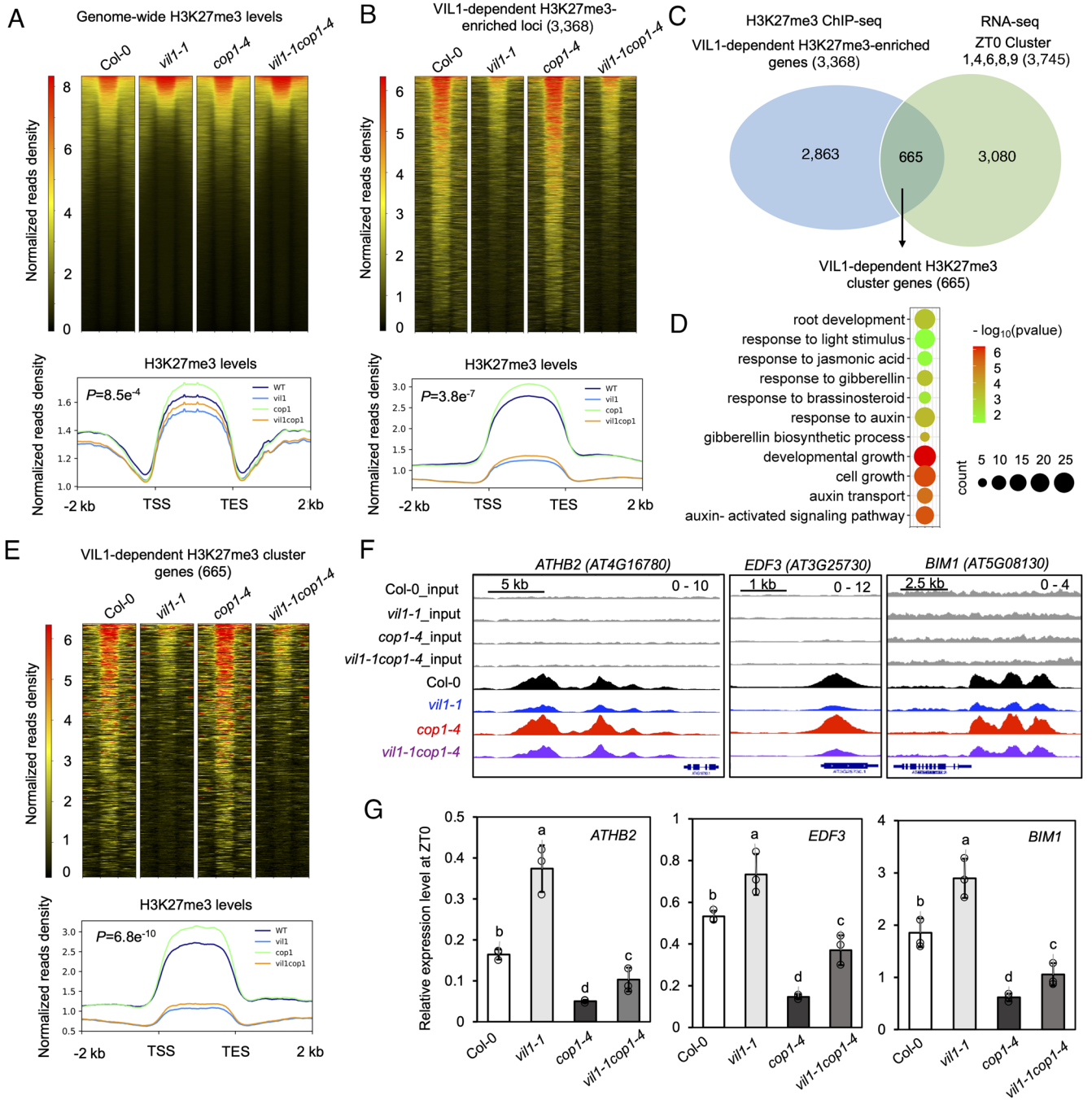

Fig. 3. COP1 and VIL1 control the H3K27me3 level. (*A*) Heatmap (*Upper*) representing genome-wide H3K27me3 enrichment levels from 2 kb upstream of the transcription start site (TSS) to 2 kb downstream of the transcription end site (TES) in Col-0, *vil1-1*, *cop1-4*, and *vil1-1cop1-4*. Gradient colors represent enrichment levels. The red and dark rows indicate H3K27me3 enrichment at high and low levels, respectively. Average density plots (*Lower*) representing the distribution profiles of H3K27me3 for genome-wide loci. The *P*-value was calculated between *cop1-4* and WT in a window from 2 kb upstream to TES by Welch's *t* test. (*B*) Heatmap (*Upper*) representing H3K27me3 enrichment levels from 2 kb upstream of the TSS to 2 kb downstream of the TES of VIL1-dependent H3K27me3-enriched loci in Col-0, *vil1-1*, *cop1-4*, and *vil1-1cop1-4*. Gradient colors represent enrichment levels. The red and dark rows indicate H3K27me3 enrichment at high and low levels, respectively. Average density plots (*Lower*) representing the distribution profiles of H3K27me3 for VIL1-dependent H3K27me3-enriched genes. The *P*-value was calculated between *cop1-4* and WT in a window from 2 kb upstream to TES by Welch's *t* test. (*C*) Venn diagram shows 3,368 genes in VIL1-dependent H3K27me3-enriched loci, 3,745 genes in clusters 1, 4, 6, 8, and 9 from the hierarchical cluster analysis (*SI Appendix*, Fig. S7 *B* and *C*), and 665 VIL1-dependent H3K27me3 cluster genes. (*D*) Gene ontology (GO) analysis of 665 VIL1-dependent H3K27me3 cluster genes. For each point, the size is proportional to the number of genes, and the colors represent the *P*-value. (*E*) Heatmap (*Upper*) representing H3K27me3 enrichment levels from 2 kb upstream of the TSS to 2 kb downstream of the TES of 665 VIL1-dependent H3K27me3 cluster genes in Col-0, *vil1-1*, *cop1-4*, and *vil1-1cop1-4*. Gradient colors represent enrichment levels. The red and dark rows indicate H3K27me3 enrichment at high and low levels, respectively. Average density plots (*Lower*) representing the distribution profiles of H3K27me3 for 665 VIL1-dependent H3K27me3 cluster genes. The *P*-value was calculated between *cop1-4* and WT in a window from 2 kb upstream to TES by Welch's *t* test. (*F*) IGV screenshots show the distribution of H3K27me3 enrichment levels at *ATHB2*, *EDF3*, and *BIM1* loci. (*G*) mRNA expression of *ATHB2*, *EDF3* and *BIM1* in Col-0, *vil1-1*, *cop1-4*, and *vil1-1cop1-4* seedlings grown for 7 d in SD. Samples were collected at ZT0. The expression levels were normalized to that of *PP2A*. Error bars indicate SD, $n = 3$, biological replicates (each biological replicate is an average value of four technical replicates). The letters above each bar indicate statistical differences between the genotypes by the one-way ANOVA followed by the Tukey HSD test for multiple comparisons ($P < 0.05$).

depends on the presence of VIL1 as *vil1-1cop1-4* double mutants abolish the H3K27me3 increase in the *cop1-4* mutant (Fig. 3*A*). We further defined VIL1-dependent H3K27me3-enriched regions through the identification of loci with lower levels of H3K27me3 peaks in *vil1-1* mutants compared to WT and identified 3,368 genes as VIL1-dependent H3K27me3-enriched loci (Fig. 3*B* and Dataset S3). The overall level of H3K27me3 at VIL1-dependent H3K27me3 loci is significantly higher in the *cop1-4* mutant (Fig. 3*B*; $P = 3.8e^{-7}$), confirming that COP1 limits the H3K27me3 deposition at these loci.

Out of the 3,368 genes present in VIL1-dependent H3K27me3 loci, a total of 665 genes belong to clusters 1, 4, 6, 8, and 9 that are co-regulated by VIL1 and COP1 from the hierarchical cluster analysis. (Fig. 3*C* and *SI Appendix*, Fig. S7 *B* and *C* and Dataset S4). GO-term analysis of these genes shows that they are enriched with genes involved in responses to light and various hormones and those related to growth (Fig. 3*D*). Moreover, these genes are enriched with H3K27me3 and the level of H3K27me3 is highly elevated in the *cop1-4* mutant in a VIL1-dependent manner (Fig. 3*E*; $P = 6.8e^{-10}$). This group includes several genes, such as *ATHB2*, *EDF3*, and *BIM1,* well known for their growth-promoting function (32–36). These genes are enriched with H3K27me3 in a VIL1-dependent manner and the level of H3K27me3 is higher in the *cop1-4* mutant (Fig. 3*F*). Their mRNA expression patterns correlate with the growth behavior of the mutants (Fig. 3*G*). Taken together, our findings show that COP1 limits the deposition of H3K27me3 through the degradation of VIL1. It is interesting to note that H3K27me3 peaks at *ATHB2* and *BIM1* are observed in the intergenic regions (Fig. 3*F*), implying the presence of *cis*-regulatory elements. Indeed, H3K27me3-enriched regions of *ATHB2* coincide with the regions where chromatin loops form (21).

COP1 Limits the Deposition of H3K27me3 at Growth-Promoting Genes. We further confirmed the antagonistic relationship of COP1 and VIL1 in controlling H3K27me3 levels by chromatin immunoprecipitation followed by quantitative PCR (ChIP-qPCR) at *ATHB2, EDF3*, and *BIM1* loci (Fig. 4 *A*–*C* and *SI Appendix*, Figs. S9–S11). The levels of H3K27me3 deposition at these loci are significantly higher in the *cop1-4* mutant both at ZT0 (in dark) and ZT6 (in light) during the dark–light cycles. The H3K27me3 deposition at these loci depends on the presence of VIL1 as the H3K27me3 levels decrease significantly in both the *vil1-1* mutant and the *vil1-1cop1-4* double mutant (Fig. 4 *A*–*C* and *SI Appendix*, Figs. S9–S11). As previously reported (21), the level of H3K27me3 does not change significantly by the dark–light cycle in the WT (Fig. 4 *A*–*C*). However, the H3K27me3 enrichment at *ATHB2* is severely impaired when WT plants are kept under continuous dark conditions (*SI Appendix*, Fig. S9 *A* and *B*). Moreover, the H3K27me3 enrichment at *ATHB2* still occurs under the continuous dark condition in the *cop1-4* mutant in a VIL1-dependent manner (*SI Appendix*, Fig. S9*B*). Under the continuous light condition, the H3K27me3 enrichment at *ATHB2* occurs both in the WT and the *cop1-4* mutant at comparable levels in a VIL1-dependent manner (*SI Appendix*, Fig. S9*C*). Similar trends of the H3K27me3 enrichment at *EDF3* (*SI Appendix*, Fig. S10 *E* and *F*) and *BIM1* (*SI Appendix*, Fig. S11 *E* and *F*) loci were observed.

ATHB2 was shown to be a direct target of VIL1-phyB (21). Therefore, to address the effects of *cop1* mutations on the enrichment of VIL1 at these loci, we examined the enrichment of VIL1 (Fig. 4*D* and *SI Appendix*, Figs. S10*B* and S11*B*). The enrichment of VIL1 was observed at both the regulatory regions and the gene body regions of *ATHB2, EDF3,* and *BIM1* (Fig. 4*D* and *SI Appendix*, Figs. S10*B* and S11*B*). The VIL1 enrichment increases several folds at ZT6 compared to ZT0 in the complementation line at all tested loci, reflecting the accumulation of VIL1 protein in the light (Fig. 4*D* and *SI Appendix*, Figs. S10*B* and S11*B*). In the *cop1-4* mutant background, the level of VIL1 enrichment is higher, especially at ZT0 (Fig. 4*D* and *SI Appendix*, Figs. S10*B* and S11*B*), consistent with the increased level of VIL1 protein in *cop1-4* mutants in the dark (Fig. 1 *E* and *F*). Taken together, our data show that COP1 limits the deposition of H3K27me3 at these loci through the degradation of VIL1 in darkness.

COP1 Controls Chromatin Loop Formation at *ATHB2*. PRC2 target loci often undergo Polycomb group-dependent formation of short-distance repressive chromatin loops (37–39). The VIL1-phyB regulatory module also includes the light-dependent formation of repressive chromatin loop at the *ATHB2* locus (21). Unlike H3K27me3, which is stably maintained during the light–dark cycle, the chromatin loop at *ATHB2* is rather dynamic and is rapidly induced by light. To address the role of COP1 in mediating the formation of chromatin loop at the *ATHB2* locus, we performed chromatin conformation capture (3C) assays in Col-0, *vil1-1, cop1-4,* and *vil1-1cop1-4* backgrounds. We detected robust formation of the chromatin loop between RE1 and P2 (TSS) of the *ATHB2* locus in Col-0 (Fig. 4 *E* and *F*), as previously reported (21). Importantly, the formation of a chromatin loop at *ATHB2* significantly increases at ZT0 in the *cop1-4* mutant (Fig. 4 *E* and *F*). Therefore, COP1 functions to limit the formation of a chromatin loop at the *ATHB2* locus in the dark, likely through the degradation of VIL1 protein. Interestingly, the formation of a chromatin loop is still higher at ZT6 compared to ZT0 in the *cop1-4* mutant background, and the formation of a chromatin loop does not further increase at ZT6 in *cop1-4* mutant compared to Col-0 (Fig. 4 *E* and *F*). Therefore, other light-dependent processes, such as the accumulation of the active form of phyB, are necessary for the full extent of chromatin loop formation. Taken together, our results suggest that the increased chromatin loop levels in the dark in *cop1-4* mutants (Fig. 4 *E* and *F*) likely create chromatin architectures that favor the increased deposition of H3K27me3 (Figs. 3 and 4 *A*–*D*, and *SI Appendix*, Figs. S9–S11), contributing to the hyper-repression of growth-promoting genes (Fig. 3 *C*, *D*, and *G* and *SI Appendix*, Fig. S7).

The COP1-VIL1 Regulatory Module Functions in Parallel with HY5. COP1 is a central switch of global light-responsive gene expression in *Arabidopsis* (40). COP1 localizes into the nucleus, where it targets degradation of a long list of photomorphogenesis-promoting factors, including ELONGATED HYPOCOTYL 5 (HY5) (41–43). HY5 is a master regulator of photomorphogenesis that triggers a large number of light-dependent developmental programs upon exposure to light (44–46). Although the function of HY5 in transcriptional regulation remains elusive, a recent study showed that HY5 likely functions as a transcriptional activator by directly partnering with various light-dependent transcription factors (47). Both HY5 and VIL1 are photomorphogenesis-promoting factors and substrates of COP1 that are degraded by the UPS. *hy5* mutations also result in the partial suppression of *cop1* mutant phenotypes (48, 49), similar to *vil1* mutations (Fig. 2 *A* and *B* and *SI Appendix*, Figs. S2–S4). We included the *hy5* mutant in our RNA-seq and ChIP-seq analyses to compare the function of HY5 with that of VIL1. Consistent with the role of HY5 as a photomorphogenesis-promoting factor, our RNA-seq analysis shows that growth-promoting genes are elevated in the *hy5* mutant to a similar level to those in the *vil1* mutant (*SI Appendix*, Fig. S12*A*). However, unlike the *vil1* and the *cop1* mutants, the level of H3K27me3 at growth-promoting genes remains unaltered in the

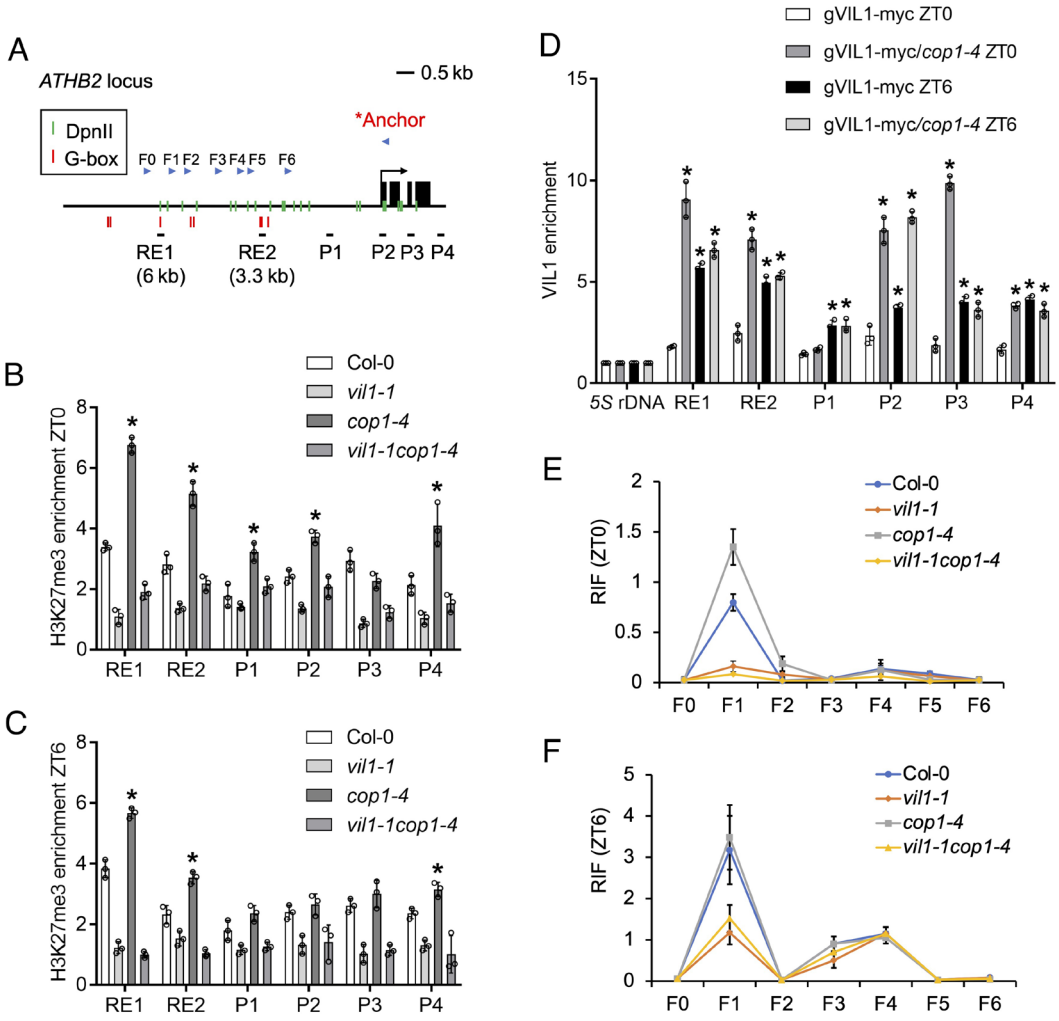

Fig. 4. COP1 controls VIL1-mediated chromatin remodeling at the *ATHB2* locus. (*A*) *ATHB2* locus, G-box elements, and ChIP–qPCR amplicons. The red vertical bars indicate predicted G-box regions. RE1, RE2, P1, P2, P3, and P4 indicate ChIP–qPCR amplicons. The green bars indicate D*pn*II enzyme sites. F0 to F6 and Anchor indicate 3C–qPCR amplicons. (*B* and *C*) H3K27me3 levels on *ATHB2* locus in Col-0, *vil1-1, cop1-4,* and *vil1-1cop1-4* at ZT0 (*B*) and ZT6 (*C*). The ChIP assays used anti-H3K27me3 antibody and anti-H3 antibody on 7-d-old seedlings grown at 22 °C under SD conditions. The *y*-axis indicates H3K27me3 enrichment relative to H3 enrichment. The error bars indicate SD ($n = 3$). The asterisks indicate statistical differences compared to the level in Col-0 in a two-tailed Student *t* test (*$P < 0.05$). (*D*) VIL1 targeting profile at the *ATHB2* locus at both ZT0 and ZT6 in the Col-0 and *cop1-4* mutant background. The ChIP assays used anti-Myc antibody on 7-d-old seedlings grown at 22 °C under SD conditions. The immunoprecipitated DNA relative to input was further normalized to that of 5*S* rDNA. The error bars indicate SD ($n = 3$). The asterisks indicate statistical differences compared to the level in gVIL1-myc ZT0 in a two-tailed Student *t* test (*$P < 0.05$). (*E* and *F*) Fold changes between the values in peaks at ZT0 and at ZT6 in the 3C assays. F sets indicate forward primer sets. Relative interaction frequency (RIF) in a 3C assay between the Anchor primer and a series of F primers in Col-0, *vil1-1*, *cop1-4*, and *vil1-1cop1-4* at ZT0 (*E*) and ZT6 (*F*). Seedlings were grown at 22 °C under SD conditions.

hy5 mutant (*SI Appendix*, Fig. S12*B*). The *hy5* mutant does not impact H3K27me3 levels at either the genomic scale or at VIL1-dependent H3K27me3 loci (*SI Appendix*, Fig. S12*C*), suggesting the distinctive mechanisms for VIL1 and HY5. Furthermore, *vil1-1hy5-215* double mutants show additive effects on hypocotyl elongation (*SI Appendix*, Fig. S13*A*), indicating that HY5 and VIL1 function independently. Moreover, no physical interaction between VIL1 and HY5 was observed in vitro pull-down assays (*SI Appendix*, Fig. S13*B*). Expression patterns of growth-promoting genes in corresponding mutants (*SI Appendix*, Fig. S13*C*) also support the notion that VIL1 and HY5 operates in parallel. Taken together, our results indicate that VIL1 serves as a substrate for COP1, affecting growth-promoting genes by triggering light-dependent chromatin remodeling independently of HY5.

Discussion

Plant growth and development are predominantly postembryonic and occur in response to environmental cues. This developmental plasticity is thought to be an adaptation to the sessile lifestyle of plants. COP1 is a central switch of global light-responsive gene expression. Our work reveals the existence of two independent modes of gene regulation by COP1. First, COP1 transcriptionally regulates the expression of a large number of genes by targeting multiple transcription factors as shown previously (4, 6, 14, 22, 40). Second, COP1 controls the expression of multiple genes especially growth-promoting genes epigenetically by targeting VIL1 in a light-dependent chromatin regulation.

Chromatin remodeling and modification are subject to massive reprogramming during many developmental transitions in eukaryotes (50). Our data show that light availability in Arabidopsis impacts the dynamic chromatin architecture changes of growth-promoting genes occurring in nuclei during seedling development. Upon light perception, VIL1 accumulates and associates with the active form of phyB, triggering chromatin remodeling, depositing H3K27me3, and thus decreasing transcriptional activity of target growth-promoting genes (Fig. 5*A*). This process is antagonized by COP1 in the dark (Fig. 5*B*). COP1 degrades VIL1 and limits the

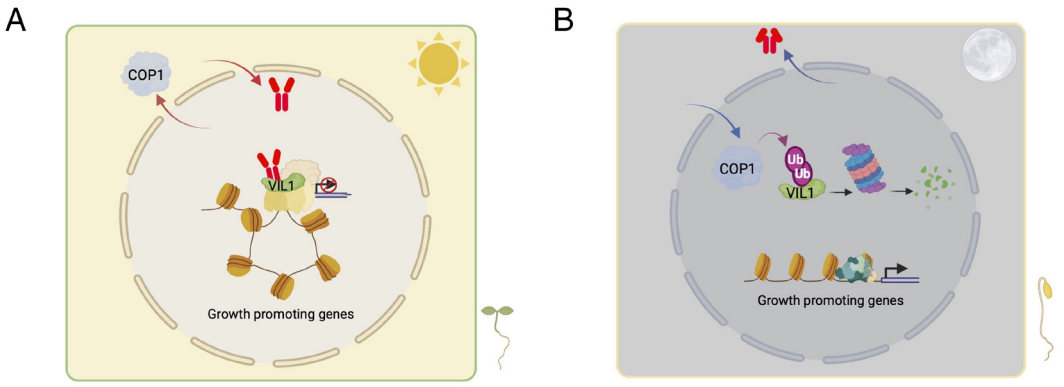

Fig. 5. COP1 controls light-dependent chromatin remodeling through VIL1. (*A*) In the light condition, COP1 is excluded and depleted in the nucleus, and VIL1 accumulates. At the same time, activated phyB (Red icon) moves into the nucleus and associates with VIL1 to trigger chromatin loop formation. VIL1 and PRC2 also deposit H3K27me3 to downstream genes. These events contribute to the repression of growth-promoting genes. (*B*) In the dark condition, the inactive form of phyB is excluded from the nucleus. COP1 accumulates in the nucleus and targets VIL1 for ubiquitination. Ubiquitinated VIL1 proteins are degraded by the 26S proteasome system. These events result in the destabilization of the chromatin loop and therefore release the repression of growth-promoting genes.

formation of chromatin loops in darkness. Concurrently in darkness, the active form of phyB dissipates in the nucleus, causing the destabilization of chromatin loops. Therefore, phyB and COP1 antagonize each other in part by affecting the formation of the VIL1-dependent chromatin loop during light–dark cycles (Fig. 5 *A* and *B*). We therefore propose that the formation of light-dependent chromatin loops by VIL1 represents a regulatory point to fine-tune desirable growth behaviors by modulating the strength of transcriptional repression via the interaction with COP1 and phyB. The involvement of chromatin regulation in light signaling provides an additional layer of regulation for effective adaptation during unpredictable environmental conditions.

Light plays a critical role in the regulation of gene expression in plants. Light-mediated chromatin regulation would allow plants to respond effectively to changes in their surroundings. Further research into the mechanisms underlying this regulation will provide important insights into the complex interplay between environmental signals, chromatin structure, and gene expression in plants. Posttranslational regulation of chromatin remodeling complexes is still poorly understood. The COP1-VIL1 regulatory module functions together with PRC2 to effectively repress gene expression. Multiple layers of regulatory modules may allow plants to exhibit plasticity to cope with changing environment.

PRC2 catalyzes H3K27me3, triggering epigenetic repression of developmentally controlled regulatory genes, which are necessary for cell identity and plasticity to promote differentiation in various eukaryotic developmental programs. The complete loss of PRC2 results in developmental arrests (51–53). VIL1, as a facultative component of PRC2, provides an access point for regulation by environmental stimuli. Here, we present the mechanism by which COP1 directly targets and degrades a component of the chromatin remodeling machinery to fine-tune gene expression and to mediate dynamic changes in chromatin architecture in response to an environmental stimulus, light.

Materials and Methods

Plant Materials and Growth Conditions. All *Arabidopsis thaliana* plants used in this study were in the Col-0 background and grown at continuous temperatures of 22 °C in a growth room with an 8-h-light/16-h-dark SD cycle. For the assays, 7-d-old seedlings were used after germination was induced at 22 °C for 24 h. The mutants *vil1-1* (SALK_136506), *cop1-4*, *cop1-6*, *phyB-9*, and *hy5-215* were used in this study. Higher-order mutants were generated by genetic crossing. *pVIL1::VIL1–myc/vil1-1* and *pVIL1::VIL1–myc/vil1-1phyB* transgenic lines were reported previously (21). The *pVIL1::VIL1–myc/vil1-1cop1-4* and *pVIL1::VIL1–myc/vil1-1cop1-4phyB* lines were generated by genetic crossing. *pVIL1::VIL1–myc* fusion was shown as *gVIL1-myc* in figures.

Measurement of Hypocotyl Lengths. For the measurement of hypocotyl length, images of 30 seedlings for each line with three independent biological replicates were taken and then measured using the publicly available ImageJ software (http://rsb.info.nih.gov/ij/). Seeds were plated on MS medium without sugar and kept in the dark for 3 d at 4 °C. Seeds were then exposed to 3 h of white light (100 μmol m^{-2} s^{-1}) to induce germination and then kept in the dark for 21 h. The dark-grown seedlings were exposed to far-red light (34 μmol m^{-2} s^{-1}) for an additional 10 min before being put in darkness. All the other plates were then placed in conditions for 3 d as described in the figures. For the measurement of hypocotyl length under short-day conditions, seeds were grown in SD for 7 d. Light fluence rates were measured using a spectroradiometer (Model EPP2000; StellarNet) as described previously (54).

Vector Constructions and Protein Purification. MBP-COP1, MBP-VIL1, and GST-HY5 were prepared as described previously (21, 27, 31, 55). For purification of GST-VIL1, *VIL1* was cloned into pGEX4T-1 using the primers listed in *SI Appendix*, Table S1. Plasmid was transformed into BL21(DE3) cells. Protein expression was induced under 16 °C overnight with 0.1 mM IPTG. Collected cells were sonicated in binding buffer (100 mM Tris-Cl, pH 7.5, 150 mM NaCl, 0.2% Tergitol NP-40, 1x Protease inhibitor cocktail, and 1 mM PMSF) and purified using GST agarose beads (Pierce, Cat. # 20211). Proteins were eluted with the elution buffer (Tris-Cl, PH 7.5, 150 mM NaCl, 1 mM, 10 mM glutathione, 10% Tergitol NP-40, 10% glycerol, 1 mM PMSF, and 1x Protease inhibitor cocktail) into separate fractions. The eluted proteins were analyzed on SDS-PAGE gel and used for pull-down and in vitro ubiquitination assay.

Protein Extraction and Western Blot Analysis. To analyze VIL1 abundance in dark-to-light and light-to-dark transitions, seeds were surface sterilized and grown in the dark or continuous white light (100 μmol m^{-2} s^{-1}) for 4 d or following the respective conditions (continues dark or light treatment, different hours of dark or light treatment, 100 μmol m^{-2} s^{-1}) as described in the figure legends. For total protein extraction, 0.1 g of whole seedlings was collected and ground in 100 μL denaturing extraction buffer [100 mM Tris pH 7.5, 1 mM EDTA, 8 M Urea, 1x protease inhibitor cocktail (Sigma-Aldrich Co., cat# 59), and 2 mM PMSF] and cleared by centrifugation at 20,200×*g* for 10 min at 4 °C. Samples were boiled for 10 min with 6X SDS sample buffer and separated on a 10% SDS-PAGE gel, blotted onto PVDF membranes, and probed with corresponding antibodies. Antibodies used in these studies are anti-Myc (Santa Cruz, c-myc (9E10) X, Cat. No: sc-40 X), anti-GFP (Abcam, Cat. # ab6556 for immunoprecipitation), and anti-Tubulin antibodies (Enzo Life Sciences, Cat. # BML-PW8770-0025). Secondary HRP-bound antibodies were visualized with Super Signal West Pico

Chemiluminescent substrate (Pierce Biotechnology Inc.) and developed with an X-ray film or GBox-F3 Syngene Imager.

The intensity of signal bands from three independent blots was quantified using ImageJ software, and the VIL1 values were divided by the Tubulin values to generate a ratio for each sample. The VIL1 level in the light was set to 1 from these ratios, respectively, and the relative values of the other time points were then calculated. These relative values were shown as line graphs in each figure in addition to the blots. The Student *t* test was used to analyze the significant difference.

Split Luciferase Assay. COP1 and VIL1 were cloned into pPZP211–nLuc and pPZP211–cLuc vectors, respectively (modified pPZP211 vectors; 35S promoter driven, N-terminal half of luciferase (nLuc) tag or C-terminal half of luciferase (cLuc) tag). Each construct was then infiltrated into *N. benthamiana* leaf epidermal cells. Three days after the infiltration, the luciferase was activated by luciferin solution (0.1% Triton X-100, 1 mM luciferin), and the signal was detected under the NightOwl II LB 983 in vivo imaging system.

In Vitro Pull-Down Assay. For in vitro pull-down assays, MBP-COP1, GST-VIL1, MBP-VIL1, and GST-HY5 fusion proteins were prepared as described previously. 1ug protein was used for each of them. All protein combinations were incubated with 20 mL of amylose resin in the binding buffer (50 mM Tris-Cl, pH 7.5, 150 mM NaCl, 0.6% Tween 20, and 1 mM DTT) for 3 h. The beads were collected and washed six times with 5 min rotation each time in a binding buffer. The bound VIL1 or HY5 were detected by anti-GST-HRP conjugate (RPN1236; GE Healthcare Biosciences). MBP-COP1 or MBP-VIL1 was detected by anti-MBP antibody (NEB, Cat. No: E8032S). Membranes were developed and visualized as described above.

In Vivo co-IP Assay. For co-IP experiments with tobacco, VIL1 and COP1 CDS were cloned into the pENTR_dTOPO vector and transferred to pEarlyGate302 vector and pB7FWG2 vector by the Gateway cloning method, respectively. Constructs were then infiltrated into *N. benthamiana* leaf epidermal cells. Three days after the infiltration, 1 g of tissue was used for total protein extraction, as described below. Total protein was incubated with Dynabeads Protein A (Life Technologies Co., Cat. No: 10002D) bound with anti-GFP antibody (ab9110; Abcam). Immuno-precipitated proteins were analyzed by immunoblotting.

For co-IP experiments with transgenic seedlings, homozygous *pVIL1::VIL1–myc/vil1-1* or *pVIL1::VIL1–myc/vil1-1phyB* transgenic seedlings were grown in the dark for 4 d and then treated with 40 μM BORTZ (LC Laboratories) for at least 4 h. Total proteins were extracted from 1 g tissue with 1 mL protein extraction buffer. After 15 min centrifugation at 16,000×*g* at 4 °C in darkness, 100 μL supernatant of each sample was reserved as total. The remainder was incubated with Dynabeads Protein G (Life Technologies Co., Carlsbad, CA, Cat. No: 10002D) bound with anti-myc antibody (Santa Cruz, c-myc (9E10) X, Cat. No: sc-40 X). Twenty microliters of Dynabeads with 1 μg antibody were used for individual samples. After 2-h incubation in the dark at 4 °C, beads were washed three times with 1 mL protein extraction buffer with 0.2% NP40. Immuno-precipitated proteins were analyzed by immunoblotting.

In Vitro Ubiquitination Assay. The GST-VIL1 and MBP-COP1 were prepared as described previously. UBE1 (E1), UbcH5b (E2), and Flag-tagged ubiquitin (Flag-Ub) were obtained commercially (Boston Biochem, Cambridge, MA, USA). All in vitro ubiquitination assay procedures were performed as described (9, 31, 56). Briefly, 5 μg of FLAG-ubiquitin, 25 ng of E1, 100 ng of E2, 600 ng of MBP-COP1, and 400 ng of GST-VIL1 were used in the reaction. The reaction mixture was incubated for 2 h at 30 °C. Reaction was attenuated by the addition of 1x SDS sample buffer and boiling at 95 °C for 5 min. Proteins were separated onto 6.5% SDS-PAGE and transferred to PVDF membranes. Blots were probed with anti-GST-HRP conjugate (GE Healthcare Biosciences, Pittsburgh, PA, USA) to detect GST-VIL1. Moreover, blots were also probed with anti-Flag (Sigma-Aldrich Co. Cat. No: F1804) antibody to detect ubiquitylated VIL1 protein.

Y2H Analyses. For GAL4 system Y2H assays, VIL1 and COP1 CDS were cloned into the pENTR_dTOPO vector and transferred to pDEST22 vector and pDEST32 vector as AD-fusion and BD-fusion constructions by the Gateway cloning method, respectively. Primers are listed in *SI Appendix*, Table S1. Different combinations of prey and bait constructs were transformed into the yeast strain, EH109, and selected on -Leu, -Trp, -His medium at 30 °C for 3 to 4 d.

For quantitative β-galactosidase assays, the clonings of the full-length, different truncated forms and mutant versions of COP1 have been described previously (31). The full-length and various truncated forms of VIL1 were PCR amplified using the primers listed in *SI Appendix*, Table S1. The PCR product and the vector pEG202 were digested with EcoRI restriction enzyme and then ligated to produce BD-fusion constructs. All the constructs were verified by restriction enzyme digestion and sequencing. For the Y2H assays, different combinations of prey and bait constructs were transformed into the yeast strain, EGY48-0, and selected on -His, -Ura, -Trp minimal synthetic medium at 30 °C for 3 to 4 d. The quantitative β-galactosidase assay was performed according to the manufacturer's instructions (Matchmaker Two-Hybrid System, Clontech Laboratories Inc.). Three independent repeats were performed for the β-galactosidase assays, and the average values are shown with SD.

RNA Isolation, RT-PCR, and Quantitative RT-PCR Assays. Total RNA was isolated from materials indicated in the figure legends using the Sigma-Aldrich plant RNA isolation kit as described (57). One microgram of total RNA was reverse transcribed using SuperScript III (Invitrogen) as described in the manufacturer's protocol. For the RT-PCR, gene-specific primers listed in *SI Appendix*, Table S1 were used to detect mRNA levels. *PP2A* (At1g13320) was used as a control for the normalization of the expression data. Real-time PCR was performed using the Power SYBR Green RT-PCR Reagents Kit (Applied Biosystems) in a 7900HT Fast Real-Time PCR machine (Applied Biosystems).

RNA-seq. Whole seedlings grown on MS medium under short-day conditions were collected at zeitgeber time (ZT) 0. Each sample has three replicates. Total RNAs were extracted using TRIzol (Invitrogen) and treated with DNase I (Promega) to eliminate traces of genomic DNA. Sequencing libraries were prepared with 500 ng total RNA following NEBNext Poly(A) mRNA Magnetic Isolation Module (NEB #E7420). Libraries were assessed on a bioanalyzer (Agilent High Sensitivity DNA Assay) and sequenced on Illumina NextSeq 500 platform. RNA-seq clean reads were aligned to TAIR10 genome release using HISAT2 with default parameters. Gene expression was quantified as counts per million reads mapped (CPM). Differentially expressed genes were determined with edgeR over three biological replicates. Genes relative to Col-0 and FDR < 0.05 were considered as DEGs. GO term enrichment was performed over the sets of DEGs with the online tools (http://geneontology.org).

ChIP-qPCR Assay. Three biological replicates of seedlings indicated in the figure legends grown in a short-day condition for 7 d and collected at ZT times were used for ChIP-qPCR analysis. The ChIP experiment was performed as previously described (58). Anti-Myc (Santa Cruz, c-myc (9E10) X, Cat. No: sc-40 X) and anti-H3K27me3 (Millipore, Cat. No: 07-449) antibodies were used for immunoprecipitation. After elution, reversing cross-links, and DNA purification, the amount of each precipitated DNA fragment was detected by real-time qPCR using specific primers listed in *SI Appendix*, Table S1. Three biological replicates were performed, and three technical repeats were carried out for each biological replicate. The Student *t* test was used to analyze the significant difference.

H3K27me3 ChIP-seq. H3K27me3 ChIP-seq assays were conducted by using Col-0, *vil1-1*, *cop1-4*, and *vil1-1cop1-4* mutants. Whole seedlings grown on MS medium under short-day conditions were collected at zeitgeber time (ZT) 0. Three biological replicates with one input for each genotype were prepared for sequencing. ChIP-seq libraries were prepared using the NEBNext ChIP-seq Library Prep Kit and sequenced on an Illumina NextSeq 500 platform. Sequencing reads were mapped to the Arabidopsis reference genome (TAIR10) with Bowtie2. Peak calling used MACS2 and applied q < 0.01. The Diffbind package was used for the differential peak analysis with thresholds < 0.05. Mapped reads were normalized using deepTools and visualized using IGV.

3C Assay. 3C experiment was performed as previously described (21). Seedlings were cross-linked in 2% formaldehyde for 30 min (10 min, break, 10 min, break, 10 min) and then quenched by adding glycine (final, 0.125 M) under a vacuum for 5 min. The seedlings were collected and finely ground in liquid nitrogen. The nuclei were isolated, and the chromatin was digested by DpnII restriction enzyme (NEB; R0543M; size, 5,000 units) at 37 °C overnight. For ligation, T4 DNA ligase (NEB; M0202M; size, 100,000 units) was treated for 5 h at 16 °C and 2 h at room temperature. The ligated

DNA was purified by phenol/chloroform/isoamyl-alcohol (25:24:1) extraction and ethanol precipitation. Quantitative PCR was performed to calculate the RIFs. The specific primer sets used in the 3C–qPCR analysis are listed in *SI Appendix*, Table S1.

Data, Materials, and Software Availability. Original raw sequencing reads are deposited in SRA under accession number GSE233273 (59). All other data are included in the manuscript and/or supporting information.

ACKNOWLEDGMENTS. We acknowledge the Texas Advanced Computing Center (http://www.tacc.utexas.edu) at The University of Texas at Austin for providing High Performance Computing resources that have contributed to the research results reported within this paper. We wish to thank Dr. Richard Amasino for comments on the manuscript and Dr. Ryan Kirkbride and Dr. Xianqiang Wang for advice on sequencing analysis. This work was supported by NIH R01GM100108 and NSF IOS 1656764 to S.S., and MCB 2014408 to E.H.

1. X.-W. Deng *et al.*, COP1, an Arabidopsis regulatory gene, encodes a protein with both a zinc-binding motif and a Gβ homologous domain. *Cell* **71**, 791–801 (1992).
2. J. C. Marine, Spotlight on the role of COP1 in tumorigenesis. *Nat. Rev. Cancer* **12**, 455–464 (2012).
3. R. Podolec, R. Ulm, Photoreceptor-mediated regulation of the COP1/SPA E3 ubiquitin ligase. *Curr. Opin. Plant Biol.* **45**, 18–25 (2018).
4. O. S. Lau, X. W. Deng, The photomorphogenic repressors COP1 and DET1: 20 years later. *Trends Plant Sci.* **17**, 584–593 (2012).
5. J. Ponnu, U. Hoecker, Signaling mechanisms by Arabidopsis cryptochromes. *Front. Plant Sci.* **13**, 844714 (2022).
6. X. Han, X. Huang, X. W. Deng, The photomorphogenic central repressor COP1: Conservation and functional diversification during evolution. *Plant Commun.* **1**, 100044 (2020).
7. M. T. Osterlund, X. W. Deng, Multiple photoreceptors mediate the light-induced reduction of GUS-COP1 from Arabidopsis hypocotyl nuclei. *Plant J.* **16**, 201–208 (1998).
8. D. J. Sheerin *et al.*, Light-activated phytochrome A and B interact with members of the SPA family to promote photomorphogenesis in Arabidopsis by reorganizing the COP1/SPA complex. *Plant Cell* **27**, 189–201 (2015).
9. Y. Saijo *et al.*, The COP1–SPA1 interaction defines a critical step in phytochrome A-mediated regulation of HY5 activity. *Genes Dev.* **17**, 2642–2647 (2003).
10. M. C. Cheng, P. K. Kathare, I. Paik, E. Huq, Phytochrome signaling networks. *Annu. Rev. Plant Biol.* **72**, 217–244 (2021).
11. J.-H. Jung *et al.*, Phytochromes function as thermosensors in Arabidopsis. *Science* **354**, 886–889 (2016).
12. M. Legris *et al.*, Phytochrome B integrates light and temperature signals in Arabidopsis. *Science* **354**, 897–900 (2016).
13. A. G. von Arnim, X. W. Deng, Light inactivation of Arabidopsis photomorphogenic repressor COP1 involves a cell-specific regulation of its nucleocytoplasmic partitioning. *Cell* **79**, 1035–1045 (1994).
14. U. Hoecker, The activities of the E3 ubiquitin ligase COP1/SPA, a key repressor in light signaling. *Curr. Opin. Plant Biol.* **37**, 63–69 (2017).
15. S. Sung, R. M. Amasino, Vernalization in *Arabidopsis thaliana* is mediated by the PHD finger protein VIN3. *Nature* **427**, 159–164 (2004).
16. S. Sung, R. J. Schmitz, R. M. Amasino, A PHD finger protein involved in both the vernalization and photoperiod pathways in Arabidopsis. *Genes Dev.* **20**, 3244–3248 (2006).
17. T. Greb *et al.*, The PHD finger protein VRN5 functions in the epigenetic silencing of Arabidopsis FLC. *Curr. Biol.* **17**, 73–78 (2007).
18. D.-H. Kim, S. Sung, Coordination of the vernalization response through a VIN3 and FLC gene family regulatory network in Arabidopsis. *Plant Cell* **25**, 454–469 (2013).
19. W. Zong, J. Kim, Y. Bordiya, H. Qiao, S. Sung, Abscisic acid negatively regulates the Polycomb-mediated H3K27me3 through the PHD-finger protein, VIL1. *New Phytol.* **235**, 1057–1069 (2022).
20. J. Kim *et al.*, Warm temperature-triggered developmental reprogramming requires VIL1-mediated, genome-wide H3K27me3 accumulation in Arabidopsis. *Development* **150**, dev201343 (2023).
21. J. Kim *et al.*, Phytochrome B triggers light-dependent chromatin remodelling through the PRC2-associated PHD finger protein VIL1. *Nat. Plants* **7**, 1213–1219 (2021).
22. J. Ponnu, U. Hoecker, Illuminating the COP1/SPA ubiquitin ligase: fresh insights into its structure and functions during plant photomorphogenesis. *Front. Plant Sci.* **12**, 662793 (2021).
23. W. Wang, Q. Chen, J. R. Botella, S. Guo, Beyond light: insights into the role of constitutively photomorphogenic1 in plant hormonal signaling. *Front. Plant Sci.* **10**, 557 (2019).
24. P. Wang *et al.*, COR27 and COR28 encode nighttime repressors integrating Arabidopsis circadian clock and cold response. *J. Integr. Plant Biol.* **59**, 78–85 (2017).
25. E. González-Grandío *et al.*, Chromatin changes in phytochrome interacting factor-regulated genes parallel their rapid transcriptional response to light. *Front. Plant Sci* **13**, 803441 (2022).
26. B. C. Willige *et al.*, PHYTOCHROME-INTERACTING FACTORs trigger environmentally responsive chromatin dynamics in plants. *Nat. Genet.* **53**, 955–961 (2021).
27. W. Wang *et al.*, Direct phosphorylation of HY5 by SPA kinases to regulate photomorphogenesis in Arabidopsis. *New Phytol.* **230**, 2311–2326 (2021).
28. M. C. Cheng *et al.*, PCH1 and PCHL directly interact with PIF1, promote its degradation, and inhibit its transcriptional function during photomorphogenesis. *Mol. Plant* **13**, 499–514 (2020).
29. J. Adams, M. Kauffman, Development of the proteasome inhibitor Velcade™(Bortezomib). *Cancer Investig.* **22**, 304–311 (2004).
30. X. W. Deng, P. H. Quail, Genetic and phenotypic characterization of cop1 mutants of *Arabidopsis thaliana*. *Plant J.* **2**, 83–95 (1992).
31. X. Xu *et al.*, PHYTOCHROME INTERACTING FACTOR1 enhances the E3 ligase activity of CONSTITUTIVE PHOTOMORPHOGENIC1 to synergistically repress photomorphogenesis in Arabidopsis. *Plant Cell* **26**, 1992–2006 (2014).
32. O. Cassan *et al.*, A gene regulatory network in Arabidopsis roots reveals features and regulators of the plant response to elevated CO(2). *New Phytol.* **239**, 992–1004 (2023), 10.1111/nph.18788.
33. T. Liang *et al.*, UVR8 interacts with BES1 and BIM1 to regulate transcription and photomorphogenesis in Arabidopsis. *Dev. Cell* **44**, 512–523.e515 (2018).
34. Y. Yin *et al.*, A new class of transcription factors mediates brassinosteroid-regulated gene expression in Arabidopsis. *Cell* **120**, 249–259 (2005).
35. A. Kunihiro *et al.*, PHYTOCHROME-INTERACTING FACTOR 4 and 5 (PIF4 and PIF5) activate the homeobox ATHB2 and auxin-inducible IAA29 genes in the coincidence mechanism underlying photoperiodic control of plant growth of *Arabidopsis thaliana*. *Plant Cell Physiol.* **52**, 1315–1329 (2011).
36. C. Yang *et al.*, PIF7-mediated epigenetic reprogramming promotes the transcriptional response to shade in Arabidopsis. *EMBO J.* **42**, e111472 (2023).
37. D. H. Kim, S. Sung, Vernalization-triggered intragenic chromatin loop formation by long noncoding RNAs. *Dev. Cell* **40**, 302–312.e304 (2017).
38. C. Lanzuolo, V. Roure, J. Dekker, F. Bantignies, V. Orlando, Polycomb response elements mediate the formation of chromosome higher-order structures in the bithorax complex. *Nat. Cell Biol.* **9**, 1167–1174 (2007).
39. K. P. Eagen, E. L. Aiden, R. D. Kornberg, Polycomb-mediated chromatin loops revealed by a subkilobase-resolution chromatin interaction map. *Proc. Natl. Acad. Sci. U.S.A.* **114**, 8764–8769 (2017).
40. L. Ma *et al.*, Genomic evidence for COP1 as a repressor of light-regulated gene expression and development in Arabidopsis. *Plant Cell* **14**, 2383–2398 (2002).
41. M. T. Osterlund, N. Wei, X. W. Deng, The roles of photoreceptor systems and the COP1-targeted destabilization of HY5 in light control of Arabidopsis seedling development. *Plant Physiol.* **124**, 1520–1524 (2000).
42. P. D. Duek, M. V. Elmer, V. R. van Oosten, C. Fankhauser, The degradation of HFR1, a putative bHLH class transcription factor involved in light signaling, is regulated by phosphorylation and requires COP1. *Curr. Biol.* **14**, 2296–2301 (2004).
43. J. Yang *et al.*, Repression of light signaling by Arabidopsis SPA1 involves post-translational regulation of HFR1 protein accumulation. *Plant J.* **43**, 131–141 (2005).
44. Y. Xiao *et al.*, HY5: A pivotal regulator of light-dependent development in higher plants. *Front. Plant Sci.* **12**, 800989 (2021).
45. S. N. Gangappa, J. F. Botto, The multifaceted roles of HY5 in plant growth and development. *Mol. Plant* **9**, 1353–1365 (2016).
46. A. Bhatnagar, S. Singh, J. P. Khurana, N. Burman, Biotechnology, HY5-COP1: The central module of light signaling pathway. *J. Plant Biochem.* **29**, 590–610 (2020).
47. Y. Burko *et al.*, Chimeric activators and repressors define HY5 activity and reveal a light-regulated feedback mechanism. *Plant Cell* **32**, 967–983 (2020).
48. C. Bourbousse *et al.*, Light signaling controls nuclear architecture reorganization during seedling establishment. *Proc. Natl. Acad. Sci. U.S.A.* **112**, E2836–E2844 (2015).
49. L.-H. Ang, X.-W. Deng, Regulatory hierarchy of photomorphogenic loci: Allele-specific and light-dependent interaction between the HY5 and COP1 loci. *Plant Cell* **6**, 613–628 (1994).
50. G. Perrella *et al.*, Let it bloom: Cross-talk between light and flowering signaling in Arabidopsis. *Physiol. Plant.* **169**, 301–311 (2020).
51. A. Förderer, Y. Zhou, F. Turck, The age of multiplexity: Recruitment and interactions of Polycomb complexes in plants. *Curr. Opin. Plant Biol.* **29**, 169–178 (2016).
52. I. Mozgova, L. Hennig, The polycomb group protein regulatory network. *Annu. Rev. Plant. Biol.* **66**, 269–296 (2015).
53. U. Grossniklaus, R. Paro, Transcriptional silencing by polycomb-group proteins. *Cold Spring Harb. Perspect. Biol.* **6**, a019331 (2014).
54. H. Shen, J. Moon, E. Huq, PIF1 is regulated by light-mediated degradation through the ubiquitin-26S proteasome pathway to optimize photomorphogenesis of seedlings in Arabidopsis. *Plant J.* **44**, 1023–1035 (2005).
55. I. Paik *et al.*, A phyB-PIF1-SPA1 kinase regulatory complex promotes photomorphogenesis in Arabidopsis. *Nat. Commun.* **10**, 4216 (2019).
56. H. S. Seo *et al.*, LAF1 ubiquitination by COP1 controls photomorphogenesis and is stimulated by SPA1. *Nature* **423**, 995–999 (2003).
57. V. N. Pham, P. K. Kathare, E. Huq, Dynamic regulation of PIF 5 by COP 1–SPA complex to optimize photomorphogenesis in Arabidopsis. *Plant J.* **96**, 260–273 (2018).
58. E. Shor, I. Paik, S. Kangisser, R. Green, E. Huq, PHYTOCHROME INTERACTING FACTORS mediate metabolic control of the circadian system in Arabidopsis. *New Phytol.* **215**, 217–228 (2017).
59. W. Wang, J. Kim, T. S. Martinez, E. Huq, S. Sung, COP1 controls light-dependent chromatin remodeling in Arabidopsis. Gene Expression Omnibus. https://www.ncbi.nlm.nih.gov/geo/query/acc.cgi?acc=GSE233273. Deposited 23 May 2023.